Effect of the Split-Ring Resonator Width on the Microwave Microplasma Properties

Roberto A. Dextre and Kunning G. Xu, *Member, IEEE*

Abstract—In this paper, a microstrip split-ring resonator microwave-induced plasma source was developed and the effect of the resonator strip width on the microplasma properties was studied. The end-goal of this paper is to implement the resonator into an in-space micropropulsion system. We thus need to understand the behavior of the microplasma to optimize the thruster performance. A range of resonators with widths from 1.5 to 6 mm were designed to generate a microplasma in argon. Simulations of the electric fields were performed to determine the peak gap electric field. Single Langmuir probe measurements were taken at a pressure of 1 torr to obtain the plasma density and electron temperature. The microwave power was varied from 4.7 to 11.34 W (37–41 dBm). The simulations showed that with an increase in the microstrip width, the maximum electric field strength is obtained for the 3-mm-wide resonator. The electron temperature is also the highest for the 3-mm-wide resonator sitting at ~5.6 eV with 11.34 W of power. However, the maximum plasma density was obtained for the 1.5-mm resonator, ~1.6×10^{17}/m^3. There is an indirect relationship between the resonator electric field and the resulting microplasma properties. A theoretical analysis of a resonator-based miniature ion engine showed similar performance to the existing miniature ion engines.

Index Terms—Microplasma, propulsion, split-ring resonator (SRR).

I. INTRODUCTION

MICROPLASMA is a regime of plasma discharges where at least one dimension is confined to millimeter or smaller scales. Microplasma discharges can be formed in a variety of configurations and from vacuum to atmospheric or higher pressures. Microplasmas have a range of potential applications, including bacteria sterilization [1], [2], skin tissue treatment [3], surface activation [2], nanomaterial synthesis [4], and thin film coating [5]. This project seeks to implement microplasmas for space micropropulsion [6]. The configuration used in this paper is the split-ring resonator (SRR) microstrip. In this design, electromagnetic fields around 1 GHz are transferred into a small air gap (approximately 500 micrometer) via an SMA connector connected to the microstrip and rear ground plane. The microwave signal travels through the ring of the microstrip to the gap where a strong electric field is formed that ionizes the surrounding gas and generates the microplasma. Previous research in

SRR geometry has examined the effect of changing the air gap distance for a single SRR [7] and the interring spacing when utilizing concentric SRRs [7]. It has been understood that these changes can effect microplasma properties [8]. This research focuses on the width of a single SRR microstrip itself while holding a constant gap distance. Previous researchers have shown that the discharge gap and frequency are the primary design factors when developing an SRR [6]. The electron temperature and plasma density are measured using Langmuir probes. The experimental results are then compared with an electric field model of the SRR.

There are a number of existing microthruster concepts for small satellites [9]–[15]; however, the microwave SRR microplasma design proposed here presents a novel concept that is simple, low cost, and lightweight. Micropropulsion for small satellites can improve mission capabilities and lead to shorter spacecraft and mission development periods [16]. Other micropropulsion systems, such as the Miniature Xenon Ion thruster (MiXI) with a 3-cm-diameter discharge chamber, demonstrated a thrust level over 1.5 mN and an I_{sp} of 3184 s with 40 W of power [17]. The μ1 ion thruster, with a 2-cm discharge chamber, performs at ~0.3 mN, 1100-s I_{SP}, and 15.1 W of total power consumption [17]. The goal is to develop an SRR-based thruster at a competitive level. In order to implement the SRR into a thruster design, it is necessary to optimize the SRR source and understand the behavior of the resulting microplasma. This paper thus focuses on the effect of SRR width on the microplasma properties, density, and electron temperature, for a range of input powers. The properties are then used to calculate the theoretical performance of a miniature electrostatic ion thruster utilizing the SRR microplasma.

II. EXPERIMENT

A. Resonator Device Characteristics and Fabrication

The SRR is fabricated with photolithography and wet etching techniques using an RT/Duroid 6010 laminate as the substrate. The 6010 Duroid has a dielectric constant of ~10.2 and has a thin film of 34-μm-thick copper cladding on both sides. The SRR is created on one side of the substrate while the back plane is untouched. The central conductor of an SMA connector is soldered to the ring while the grounded body is soldered to the back plane. Fig. 1 provides a generic schematic of the SRR and it shows a fabricated SRR source with a 1.5 mm width.

A brief overview of the theoretical design of an SRR is given in the following for completeness. Further details can
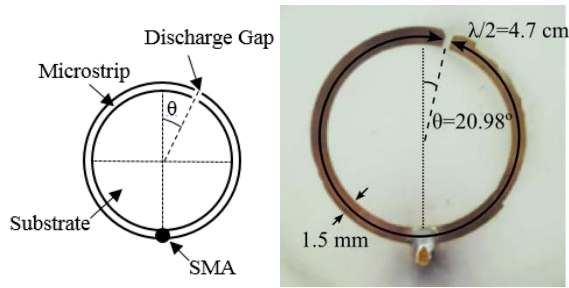
Fig. 1. Generic schematic of the SRR and a photo of the 1.5-mm SRR device with dimensions. The characteristic half wavelength set the average circumference of the ring. The strip width was then expanded equally to create the different width SRRs.

be found in [6] and [18]. The mean circumference of the SRR is designed to be half the wavelength corresponding to the driving frequency and dielectric constant of the substrate found from

$$c = \lambda f \sqrt{\varepsilon_r}. \tag{1}$$

Here, c is the speed of light, λ is the wavelength, and ε_r is the dielectric constant of the substrate. As the microwaves propagate through the device, the dielectric allows the electromagnetic field to mainly develop between the microstrip plane and the ground plane. At the discharge gap, the voltage at either end is 180° out of phase with each other and develops a large amplitude electric field that can ionize the gas. The gap location for maximum power is determined by the phase offset angle, θ. Equation (2) shows the relationship between the offset angle, the impedances, Z, and the theoretical quality factor, Q [6], [18]. An example of the positioning of the phase angle can be seen in Fig. 1

$$\cos\theta = 1 - \frac{Z_{in}\pi}{Z_0 Q}. \tag{2}$$

Assuming that the signal input impedance (Z_{in}) is 50 Ω, the characteristic impedance (Z_0) of the antenna can be determined by the geometry of the SRR as discussed in [19]. The phase angle requires knowing the quality factor, which is given by

$$Q = \frac{\pi}{\alpha\lambda} \tag{3}$$

where α is the attenuation factor, which is the function of geometry and signal frequency. Methods for calculating the attenuation factor can be found in [19].

In this paper, SRRs with a strip width ranging from 1.5 to 6 mm were designed and developed to produce microplasmas in argon. The width of the strip is increased equally (the inner diameter is decreased and outer diameter is increased) to create the test articles. A uniform 500 micrometer discharge gap was used for all SRRs. The SRRs were initially designed for an input microwave frequency of 1000 MHz. The actual simulated resonant frequency was determined as the minimum from the S_{11} return loss plot in ANSYS High-Frequency Field Simulator (HFFS). After the devices were fabricated, the resonant frequency was experimentally found as the frequency for the maximum forward power read by a Bird 7020 power sensor. The resonant frequency for each

TABLE I
FREQUENCY, QUALITY FACTOR, AND PHASE ANGLE FOR ALL SRR WIDTHS

Width (mm)	Design Frequency (MHz)	Quality Factor	Phase Angle (deg)	Simulated Resonant Frequency (MHz)	Measured Resonant Frequency (MHz)
1.5	1000	53 ±4%	20.98 ±4%	1450	1240 ± 4%
3	1000	79	21.13	1280	1240
4.5	1000	85	23.40	1180	1173
5	1000	87	24.09	1190	1173
6	1000	90	25.39	1180	1174

TABLE II
ACTUAL IMPEDANCE VALUES

SRR Width (mm)	Actual Impedance (Ohms)	V_{gap} at 5 W (V)
1.5	30.06 ±0.002%	201.4 ±0.002%
3	37.90	276.1
4.5	23.38	224.9
5	35.63	280.9
6	29.16	258.5

SRR was constant over the power range tested (4.7–11.34 W). The simulated and measured resonant frequencies along with the appropriate quality factors and phase angles are shown in Table I.

Table II shows the actual impedance measured by a network analyzer (Advantest R3767CH) and the theoretical gap voltage for each SRR width. The gap voltage can be calculated from [6]

$$V_{gap} = 4\sqrt{\frac{Z_o Q}{\pi}}\sqrt{P_{in}}. \tag{4}$$

Representative uncertainties for the calculated and measured data in Tables I and II are displayed in the corresponding first row and are consistent for all SRR devices. These values show the systematic error of the equipment utilized for collecting these measurements.

B. Langmuir Probe Diagnostic

A Langmuir probe is used to measure the electron temperature and plasma number densities of the microplasma. The probe was built using a tungsten wire covered by an alumina shield with an exposed tip at the end. The tip has a diameter of 0.127 mm, a length of 2 mm, and the end is located ~4 mm above the center of the SRR discharge gap, similarly as the one displayed in Fig. 1. The SRR was placed vertically in the vacuum chamber with the probe horizontally held with mounting brackets. The same probe was used for all measurements and its location relative to the SRR was consistent throughout the experiments. An external bias voltage was applied to the Langmuir probe and scanned from −25 to 100 V to attract the ions or electrons to the probe.
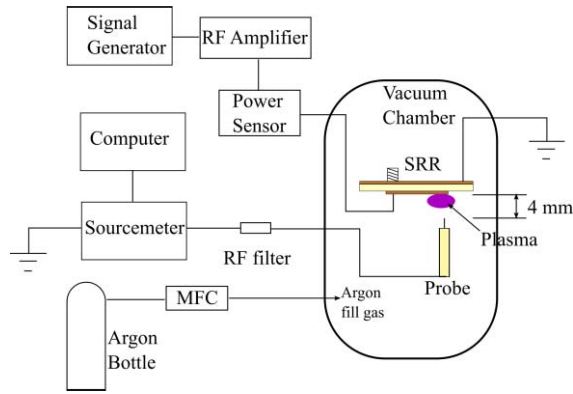
Fig. 2. Diagram of the experimental setup looking at the chamber from a top-down view.

The current at each voltage was measured and created an $I - V$ curve, which was analyzed to determine the plasma properties.

The analysis of Langmuir probe data depends on the collisionality of the plasma. The collisionality factor is defined as [20]

$$\alpha_c = \frac{\lambda_D}{\lambda_{mfp}} \qquad (5)$$

where λ_D is the Debye length and λ_{mfp} is the ion-neutral mean-free path. For argon, the simple equation $\lambda_{\mathrm{mfp}} = (330P)^{-1}$ where P is in torr and λ_{mfp} in centimeters can be used. The plasma can be considered collisional if $\alpha_c > 1$, and collisionless if $\alpha_c < 1$. The SRRs were tested at an argon pressure of 1 torr, and using both collisionless [21] and collisional methods [22] resulted in plasma properties that placed gave collisionality values from 0.00025 to 0.001, placing the plasma in the collisionless regime [22]. Thus, the collisionless Langmuir probe results were used.

The electron temperature was determined from the inverse of the slope of a plot $\ln(I_e)$ against V [20]. Equations (6) and (7) are used to calculate the electron and ion densities, respectively [21], [23]

$$I_0 = Aen_e \left(\frac{kT_e}{2\pi m} \right)^{\frac{1}{2}} \qquad (6)$$

$$I_+ = Ane \left(-\frac{e\varphi}{8M} \right)^{\frac{1}{2}}. \qquad (7)$$

Here, n_e is the electron number density, n is the ion density, I_0 is the electron saturation current, I_+ is the ion saturation current, e is the magnitude of the electronic charge, m is the electronic mass, M is the ion mass, φ is the value of the dc potential, k is Boltzmann's constant, and A is the probe area [23].

C. Experimental Setup

A schematic of the experimental setup is shown in Fig. 2. The SRRs were all tested at their resonant frequencies shown in Table I. The preamplified input power from the microwave generator ranged from -11.0 to -7.0 dBm. The power was increased by $+48$ dB by the RF amplifier, thus 37–41 dBm. A Bird 7020 power sensor measured the forward and reflected

power and the voltage standing wave ratio (VSWR) in the circuit. The VSWR measurements were used to convert the total input power to forward to the SRR. Overall, the total forward power sent to the SRR varied from 4.7 to 11.34 W. This power range was chosen based on the capabilities of the RF amplifier, the required ignition power, and the desire to run at < 15 W to meet small satellite power systems. All powers reported from here on are the forward power. Following the power sensor, the transmission line then enters the vacuum chamber and to the SRR. The SRRs were tested at a chamber pressure of 1-torr argon similar to other works [18], [24]. The signal then reaches the source and generates the argon microplasma.

Once the microplasma is generated, the Langmuir probe mounted near the gap was used to collect current measurements. A low-pass RF filter with a cutoff of 100 MHz was placed in the probe line to remove RF interference from the probe data. A LabView controlled Keithley 2410 sourcemeter was used to obtain the $I - V$ curve.

III. RESULTS AND DISCUSSION

This section presents the simulations results, the collected current–voltage data, and the resulting plasma properties. The properties of interest are the electron temperature and the electron and ion densities. The thrust and specific impulse of an ion engine can be determined theoretically from the electron temperature and the plasma densities.

A. Simulation

The electric fields in the microstrip of the SRRs were simulated with ANSYS HFFS. A higher intensity electric field should produce higher electron temperatures and plasma densities. The simulations were performed for SRR widths from 1.5 to 6 mm and power from 4.7 to 11.34 W. Only the results for the 4.7-W cases are shown here as the electric field increases linearly with power and the relationship between the SRR widths remained the same for different powers. It is noted that the meshing algorithm applied by HFSS can result in skewed measurements if the solution frequency is off the true resonant frequency. With an imperfect mesh, certain anomalies can be observed in the electric field intensity. However, it is understood that the results obtained by HFSS are approximate. Fig. 3 displays the maximum electric field strength in the microstrip along the inner edges of the discharge gap. Two example simulation results for 1.5- and 5-mm rings can be found in Fig. 4. The simulation results for all widths are located in the Appendix.

As seen from the simulation results in Fig. 3, the gap electric field has a peak at 3 mm and decreases at smaller and larger widths. There is a minor peak at 5 mm as well. This nonlinear behavior can be caused by the mismatch between the signal wavelength and the SRR width through the characteristic impedance.

The higher the combination of impedance and quality factor, the larger the voltage, and thus electric field, is achieved. However, as seen in Tables I and II, while Q increases with width, Z_o has a nonlinear behavior with the same peaks
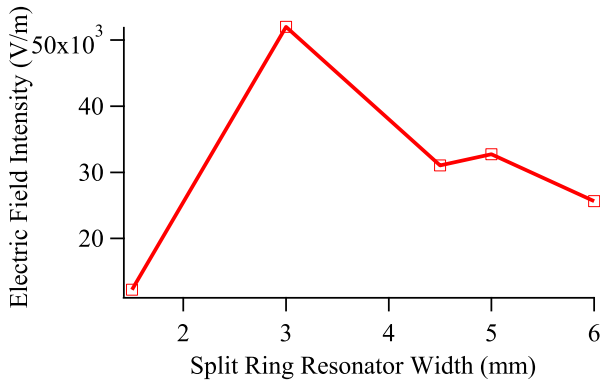
Fig. 3. Simulated electric field strength at the center of the gap versus SRR width from for 4.7 W at the resonant frequency of each device.
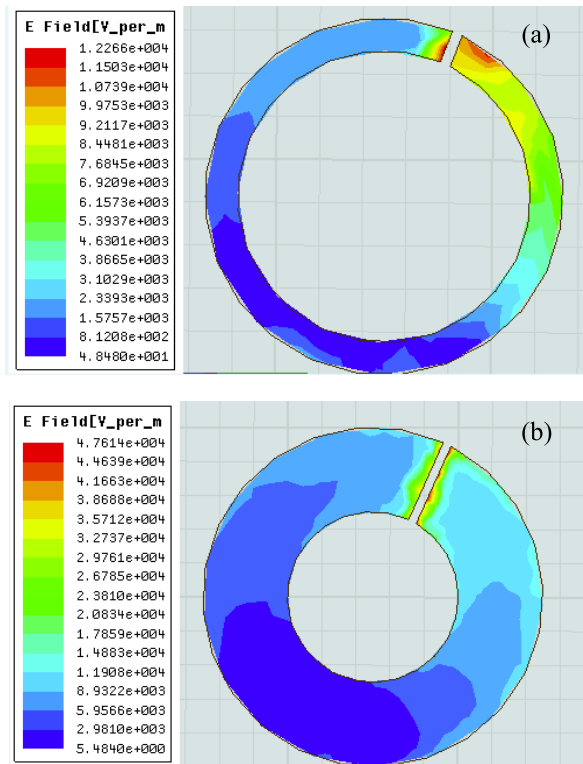

Fig. 4. SRR simulations for (a) 1.5 and (b) 5 mm widths at 4.7 W at their respective simulated resonant frequencies.

at 3 and 5 mm as the electric field strength in Fig. 3. It is known the microstrip width affects the impedance of the strip [6], and the fact is used to design stripline resonators for electronics. Control of these two parameters in SRRs to optimize the gap electric field is, however, not straightforward.

The magnitude of the electric field at the edge of the discharge gap also changes for different SRR widths. This can be primarily due to the SRR width changing the impedance of the resonator for the same input power. This impacts the magnitude of the field throughout the microstrip and it can help explain the peak at 3 mm and the significant drop in electric field between 3 and 4.5 mm in Fig. 3. It is observed that a slight increase in electric field intensity occurs at 5 mm. At the same time, the 5-mm device has a higher impedance relative to the 4.5- and 6-mm devices, as seen in Fig. 3.
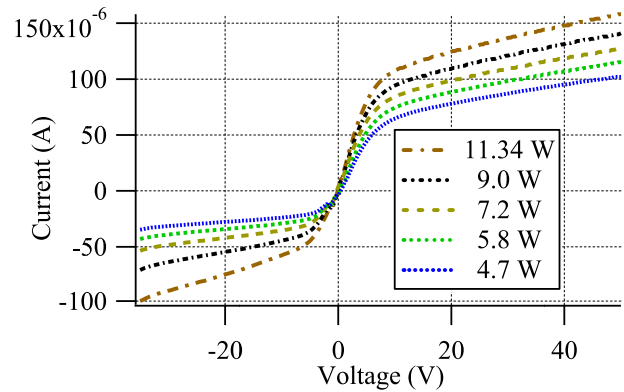

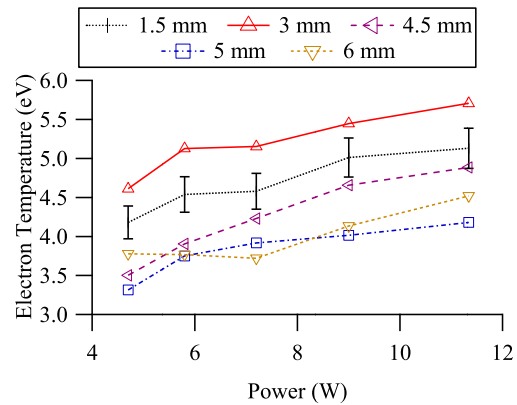Fig. 5. Current–voltage Langmuir probe curve for 1.5mm SRR.

Fig. 6. Electron temperature as a function of power for all SRR widths. 5% error bar shown on 1.5 mm.

B. Current–Voltage Curve

Fig. 5 shows a set of raw Langmuir probe $I - V$ curves for the 4.5-mm SRR over the power range tested. With an increase in power, floating potential and plasma potential become more positive. The electron retardation region also becomes steeper and the electron saturation current increases with power. This results in higher electron temperatures, which is expected for higher power. Similar curves were obtained for all SRRs tested at their respective resonant frequencies. The $I - V$ curves in Fig. 5 show that the electron saturation region occurs around 10 V and the ion saturation region around -5 V.

C. Electron Temperature

The electron temperature for each SRR as a function of power is shown in Fig. 6. The uncertainty is estimated at 5% for electron temperature, but to avoid cluttering the graphs, only one set of representative error bars is shown for the 1.5-mm case. The error bars were determined by collecting multiple $I - V$ curves at the same operating conditions (power, width, and so on), and calculating the standard deviation among the multiple sets of microplasma property data. When selecting the data for the plot $\ln(I_e)$, the specific points of the electron saturation used were varied to obtain an uncertainty due to point selection. The low noise data obtained resulted in low uncertainty by these measures. Langmuir probes can, however, have innately high uncertainty of up to 50% due to

the nature of the method and theory of analysis. However, without a second method for comparison, the innate uncertainty cannot be quantified and is taken as a uniform systematic error that does not affect the relative trends and behaviors between the different SRRs.

From Fig. 6, all devices increase in electron temperature with power and the 3-mm device had the overall highest electron temperature over the full power range, in agreement with the simulations as the 3 mm had the highest electric field intensity. With the simulation shown previously, at 4.7 W, the 5-mm device was observed to have a slight local peak. This behavior is likely due to the higher impedance in the SRR at that width. At 4.7 W, the 5 mm may have given a locally high electric field, but the electron temperature values did not agree as the 5-mm device produced some of the lowest temperatures. Conversely, the simulation showed the 1.5-mm SRR has the lowest electric field strength along the gap, but it produced the second highest electron temperatures. This discrepancy for 1.5 mm may be due to the fringing electric fields that are not captured well by the HFSS meshing algorithm. It is likely that the fringing fields play a large role in the amplification of the microplasma properties for thinner widths, but is not seen in the simulated electric fields. The higher electron temperature at 1.5 and 3 mm suggests that the electron temperature is a function of SRR width, similar to the resonant frequency, and that the trends cannot be directly predicted from field simulations. With a resonant width, optimum amplitude of the microwave signal is achieved due to better impedance matching. This leads to an increased performance of the SRR that can produce a higher electron temperature.

Observing the electron temperature in comparison to Iza and Hopwood [24], the value obtained in this research is higher. With significantly less power, ~0.5 W, the electron temperature observed is 2 eV. At 11.34 W, the electron temperature found here is 5.6 eV. This increase is expected due to the higher input power. Berglund $et\ al.$ [18] obtained an electron temperature of 2.83 eV with 4.5 W. The data obtained in this paper are proved to be in good comparison with other work.

D. Electron and Ion Densities

The electron and ion densities as a function of the forward power for each SRR are shown in Figs. 7 and 8.

The plasma densities experience a steady increase with power. Higher power produces higher electron temperatures, which increases the ionization rate. The ion density compared with electron density shows some nonquasi-neutrality, though that may be due to uncertainty in the measurement. The ion and electron densities increase at a similar rate for all widths except for 5 mm, suggesting the change in ionization rate is mostly independent of width. As seen in Figs. 7 and 8, the highest densities are achieved by the 1.5-mm SRR.

When comparing the electron temperature and plasma density of the devices, there are some discrepancies. The 1.5 mm width had the highest plasma density while the 3 mm width obtaining the highest electron temperature. The 3- and 4.5-mm SRRs achieved the second highest ion and electron number density, respectively, while the 3-mm temperatures were
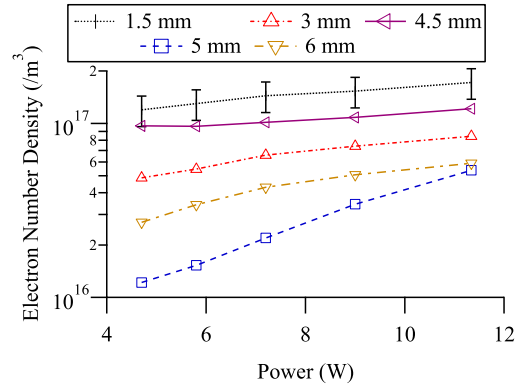

Fig. 7. Electron number density over power for all SRR designs. 20% error bar on 1.5 mm.
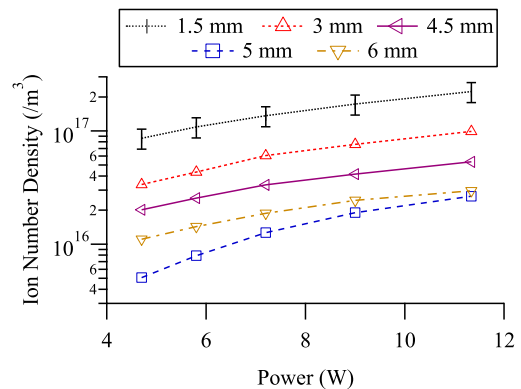

Fig. 8. Ion number density over power for all SRR designs. 20% error bar on 1.5 mm.

significantly higher than the 4.5 mm. On the other hand, the 5-mm device had the lowest density and some of the lowest recorded electron temperatures. Overall, the trend that appears to be a higher electron temperature produces a lower number density for the devices tested.

As seen by Berglund $et\ al.$ [18], an electron temperature of 2.83 eV also obtained an ion density of 5.7×10^{17}/m^3. These plasma density data are higher compared with the 1.6×10^{17}/m^3 obtained here; however, the operating frequency of Berglund is significantly higher, 2.6–2.7 GHz, which may play a role into the variations. Zhu and Pu [25], while comparing probe theory to optical emission spectroscopy, determined electron temperatures from 1 to 4 eV with an argon, xenon, and neon mixture at 13.56 MHz and 100 W. Iza and Hopwood [24] also obtained ion density measurements within the range of 2.0×10^{10}/cm^3 to 1.2×10^{11}/cm^3 with a power from 0.2 to 1.0 W. This was also accomplished at a range of pressures, from 100 to 400 mtorr.

The observations and comparisons made between the plasma properties of the various devices tested can be explained by the resonant frequency, impedance, and the other electrical properties of the SRR. As mentioned, the device is intended to be half the wavelength of the driving frequency and the input impedance into the SRR is 50 Ω from the microwave source. However, the microstrip characteristic impedance and the quality factor are a driving
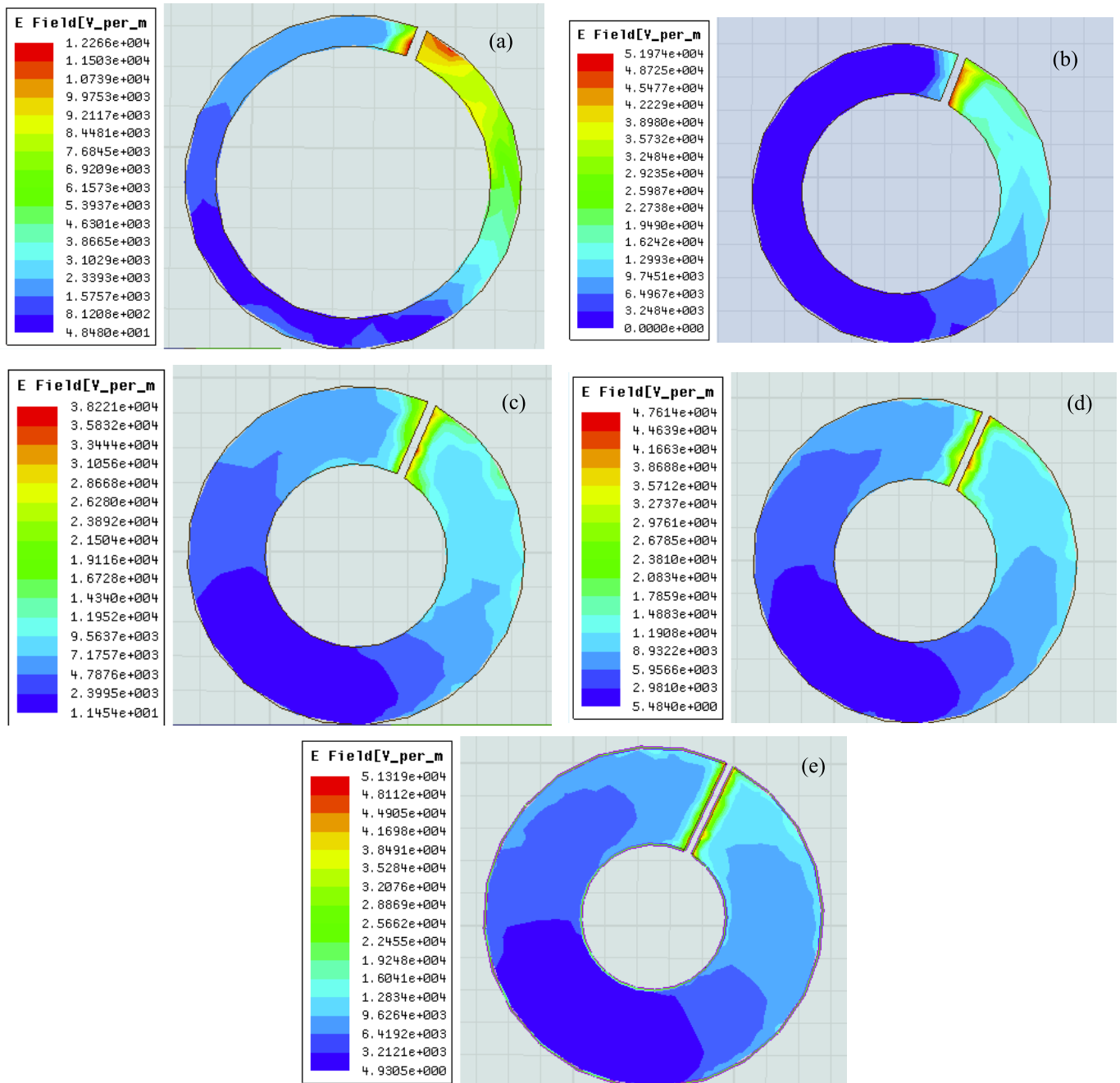
Fig. 9.   SRR EM simulations for varying widths. (a) 1.5, (b) 3, (c) 4.5, (d) 5, and (e) 6 mm.

factor in determining the voltage and thus electric field across the gap. The electric field intensity of the SRRs can be observed in Fig. 9. As SRR width increases, the characteristic impedance has a nonmonotonic behavior with highest values at 3 and 5 mm. The quality factor increases with width, but at a slow rate at large widths. The quality factor decreases in narrow microstrips due to increased conduction and radiation losses. Thus, maximizing both quality factor and impedance to improve gap voltage and presumably plasma properties is not a simple matter of increasing width to maximize quality factor.

In this experiment, the 3-mm device proved to have a higher electron temperature while the 1.5-mm device had a higher density compared with the other widths. This is mainly due to the characteristic impedance as the quality factor for the 3-mm device was lower than the larger widths. The concept of resonance plays the primary role in this paper. A resonant frequency was found and a unique quality factor was determined for each device to obtain the appropriate phase angle. Good resonant behavior is observed from the 3 mm, while the 1.5-mm device shows poor resonance, yet, obtains a higher plasma density. This may be due to the smaller widths generating a more compact plasma at a given power level. Thus, while the smaller devices had a locally higher density, the larger devices may have a higher total density but over a

larger volume. Spatial measurements are required to determine the extent of the plasma volume.

E. Miniature Ion Engine Analysis

The SRR is investigated in this paper for micropropulsion applications, specially a miniature ion engine. Other miniature ion engines have been designed using RF [10], [11], microwave [12], [13], and electron-impact ionization [14]. The SRR is an ideal candidate for miniature ion engine implementation due to its inherent small size and confined plasma volume. Using the electron temperature and plasma densities measured, with the assumption of a uniform temperature and density distribution, a theoretical performance for such a miniature ion engine can be calculated. The ion grid diameter is taken to be 3 cm, approximately equal to the mean diameter of the SRRs. The physical grid parameters, such as aperture size, grid thickness, and grid spacing, are taken from the 3-cm MiXI thruster used by Wirz [14], [17]. The aperture size for the grid sets A used by Wirz is 340 μm for the screen grid and 220 μm for the accelerator grid. The grids were developed using a 100-μm-thick molybdenum and the nominal grid spacing was 300 μm. The theoretical performance of an ion engine is given by

$$T = \gamma\, I_b \sqrt{\frac{2MV_b}{e}} = \gamma\, J_b A_g T_s \sqrt{\frac{2MV_b}{e}} \qquad (8)$$

$$I_{\mathrm{SP}} = \frac{\gamma}{g_0}\sqrt{\frac{2eV_b}{M}}. \qquad (9)$$

Here, T is thrust, I_{SP} is the specific impulse, I_b is the ion beam current, γ is the thrust correction factor that accounts for plume divergence and multiply charged ions, T_s is the screen grid transparency equal to 48.7% based on the MiXI screen grid, J_b is the current density, A_g is the area of the grid, M is the ion mass, and V_b is the beam voltage [27]. Ion engines typically have low plume divergence due to the grid alignment. We will assume a conservative $\gamma = 0.7$ and $V_b = 1000$ V for this analysis. The current density is obtained from the Bohm velocity ($J = 0.61n_0ev_B$), assuming all ions that approach the grid sheath are accelerated. The maximum thrust is produced by the 1.5-mm SRR due to its high ion density. The proposed SRR ion engine produces 0.08–0.19 mN of thrust for 4.7–11.34 W of power at a fixed 4950 s of specific impulse. The specific impulse is constant as it is mathematically a function of beam voltage, which is set at a constant 1000 V in this analysis. The thrust values are in the lower range of the similarity sized 3-cm MiXI thruster's 0.1–1.55 mN, though the specific impulse is much higher. The calculated performance does not account for ion engine operational parameters, such as perveance and net-to-voltage ratio, thus likely over predicts the real performance, especially specific impulse.

This simple analysis was also done with an argon plasma. Ion engines, such as the MiXI, typically use xenon as propellant. Xenon is heavier and has a lower ionization energy than argon. Thus, the use of xenon with the SRR could lead to higher densities and thrust but lower specific impulse. The effect of the resonator width should have similar or greater differences for xenon as the main difference between the two species is their ionization energy, which is influenced by the gap electric field.

A second consideration for an SRR-based miniature ion engine is the interaction between the SRR surface electric field and the fields generated by the ion optics. In this aspect, the proposed thruster is similar to the existing RF ion engines, such as the European RIT [28] where the ion optics do not interfere with the plasma generation. However, instead of using an external RF coil around a dielectric chamber to generate the plasma, the SRR's "coil" is inside the chamber. This creates a greatly possibility of electrical interference, though the effect should minor as the plasma facing screen grid is typical 10–20 V below the spacecraft and SRR potential. Thus, there should only be a small electric field that is generated inside the chamber to repel electrons from the grid. In addition, since the SRR surface waves are mostly confined to the ring, suitable separation between the SRR and the screen grid should prevent interference.

The results indicate that the use of the SRR for plasma generation can produce thrust on par with existing miniature ion engines and additionally removes the need for internal magnetic structure or a discharge cathode, which is a life limiter for ion engines.

Other considerations, such as the impact on the electric field due to the grid bias voltage, have not be accounted; however, an MiXI ion engine as characterized here is expected to have no impact on the performance or microplasma production of the SRR. This is primarily due to the operations of the SRR, which rely strictly on the high-frequency microwave producing a change in potential across the discharge gap confined to the device. The only known possible impact that can be induced on the microplasma of a designed SRR is the resonant frequency, input power, and reservoir pressure.

IV. CONCLUSION

The electron temperature and electron and ion density for an argon microplasma generated with variable width SRR devices were measured. With an increase in SRR width, simulations show that the 3- and 5-mm cases have the largest gap electric field intensity, which is confirmed by V_{gap} values. This is attributed to larger impedance and quality factors for these two widths. However, impedance and quality factor are not controlled independently. It is necessary to decrease SRR width in order to increase characteristic impedance, which leads to a decrease in quality factor due to radiation and conduction losses. For microstrip transmission lines, an increase in strip width leads to a decrease in characteristic impedance [6]. When analyzing a ring geometry, the impedance actually varies as seen in Table II. The balance between impedance and quality factor was found at a resonant width near 3 and 5 mm. The 3-mm case also showed the highest electron temperature, but the highest plasma density was achieved by the 1.5-mm SRR, which had the lowest simulated gap electric field. This indicates that the SRR width does play a significant role in the resulting plasma properties, but the gap electric field is not a direct predictor of the plasma behavior. The results for all widths show an increasing trend

in electron temperature and density with power. A theoretical analysis with for a miniature ion engine showed performance comparable to existing engines. The SRR is a viable candidate for in-space micropropulsion, though more work is needed to characterize the spatial distribution of the plasma and design and test of a thruster is needed.

REFERENCES

[1] K. Shimizu, M. Blajan, and T. Kuwabara, "Removal of indoor air contaminant by atmospheric microplasma," *IEEE Trans. Ind. Appl.*, vol. 47, no. 6, pp. 2351–2358, Nov./Dec. 2011.

[2] A. Mizuno, "Recent progress and applications of non-thermal plasma," *Int. J. Plasma Environ. Sci. Technol.*, vol. 3, no. 1, pp. 1–7, 2009.

[3] Y. C. Hong and H. S. Uhm, "Microplasma jet at atmospheric pressure," *Appl. Phys. Lett.*, vol. 89, no. 22, pp. 2004–2007, 2006.

[4] D. Mariotti and R. M. Sankaran, "Microplasmas for nanomaterials synthesis," *J. Phys. D, Appl. Phys.*, vol. 43, no. 32, p. 323001, Jul. 2010.

[5] J. Hopwood, F. Iza, S. Coy, and D. B. Fenner, "A microfabricated atmospheric-pressure microplasma source operating in air," *J. Phys. D, Appl. Phys.*, vol. 38, no. 11, pp. 1698–1703, Jun. 2005.

[6] F. Iza and J. Hopwood, "Split-ring resonator microplasma: Microwave model, plasma impedance and power efficiency," *Plasma Sour. Sci. Technol.*, vol. 14, no. 2, pp. 397–406, May 2005.

[7] P. J. Castro, J. J. Barroso, and J. P. L. Neto, "Experimental study on split-ring resonators with different slit widths," *J. Electromagn. Anal. Appl.*, vol. 5, no. 9, pp. 366–370, 2013.

[8] B. Wu, B. Li, T. Su, and C.-H. Liang, "Study on transmission characteristic of split ring resonator defected ground structure," *Prog. Electromagn. Res.*, vol. 50, no. 6, pp. 710–714, 2006.

[9] D. E. Clemens, "Performance evaluation of the microwave electrothermal thruster using nitrogen, simulated hydrazine, and ammonia," Ph.D. dissertation, Dept. Aerosp. Eng., Pennsylvania State Univ., State College, PA, USA, 2007.

[10] D. Feili, B. Lotz, S. Bonnet, B. K. Meyer, and H. W. Loeb, "μNRIT-2.5—A new optimized microthruster of Giessen University," in *Proc. 31st Int. Elect. Propuls. Conf.* Aug. 2009, pp. 1–9.

[11] T. A. Trudel, S. G. Bilén, and M. M. Micci, "Design and performance testing of a 1-cm miniature radio-frequency ion thruster," in *Proc. 31st Int. Elect. Propuls. Conf.*, 2009, pp. 20–25.

[12] D. P. Lubey, S. G. Bilén, M. M. Micci, and P.-Y. Taunay, "Design of the miniature microwave-frequency ion thruster," in *Proc. 32nd Int. Electr. Propuls. Conf.*, Sep. 2011, pp. 1–8.

[13] H. Koizumi and H. Kuninaka, "Performance evaluation of a miniature ion thruster μ1 with a unipolar and bipolar operation," in *Proc. 32nd Int. Elect. Propuls. Conf.*, 2011, pp. 1–10.

[14] R. Wirz, J. Polk, C. Marrese, and J. Mueller, "Experimental and computational investigation of the performance of a micro-ion thruster," in *Proc. 38th AIAA Joint Propuls. Conf.*, Indianapolis, IN, USA, 2002, paper AIAA 2002-3835.

[15] D. M. Goebel, R. E. Wirz, and I. Katz, "Analytical ion thruster discharge performance model," *J. Propuls. Power*, vol. 23, no. 5, pp. 1055–1067, 2007.

[16] Y. Takao, T. Takahashi, K. Eriguchi, and K. Ono, "Microplasma thruster for ultra-small satellites: Plasma chemical and aerodynamical aspects," *Pure Appl. Chem.*, vol. 80, no. 9, pp. 2013–2023, 2008.

[17] R. E. Wirz, "Miniature ion thrusters: A review of modern technologies and mission capabilities," in *Proc. 30th Int. Symp. Space Technol. Sci.*, 2015, pp. 1–11.

[18] M. Berglund, M. Grudén, G. Thornell, and A. Persson, "Evaluation of a microplasma source based on a stripline split-ring resonator," *Plasma Sour. Sci. Technol.*, vol. 22, no. 5, p. 055017, 2013.

[19] L. Changhong and L. Long, "A new characteristic impedance perturbation method for finding attenuation constants," *Microw. Opt. Technol. Lett.*, vol. 32, no, 4, pp. 243–245, 2002.

[20] T. E. Sheridan and J. Goree, "Collisional plasma sheath model," *Phys. Fluids B, Plasma Phys.*, vol. 3, no. 10, pp. 2796–2804, 1991.

[21] R. L. Merlino, "Understanding Langmuir probe current-voltage characteristics," *Amer. J. Phys.*, vol. 75, no. 12, p. 1078, 2007.

[22] P. R. Smy, "The use of Langmuir probes in the study of high pressure plasmas," *Adv. Phys.*, vol. 25, no. 5, pp. 517–553, 1976.

[23] T. I. Cox, V. G. I. Deshmukh, D. A. O. Hope, A. J. Hydes, N. S. J. Braithwaite, and N. M. P. Benjamin, "The use of Langmuir probes and optical emission spectroscopy to measure electron energy distribution functions in RF-generated argon plasmas," *J. Phys. D, Appl. Phys.*, vol. 20, no. 7, pp. 820–831, 2000.

[24] F. Iza and J. A. Hopwood, "Low-power microwave plasma source based on a microstrip split-ring resonator," *IEEE Trans. Plasma Sci.*, vol. 31, no. 4, pp. 782–787, Aug. 2003.

[25] X.-M. Zhu and Y.-K. Pu, "Optical emission spectroscopy in low-temperature plasmas containing argon and nitrogen: Determination of the electron temperature and density by the line-ratio method," *J. Phys. D, Appl. Phys.*, vol. 43, no. 40, p. 403001, 2010.

[26] C. Charles, "TOPICAL REVIEW: A review of recent laboratory double layer experiments," *Plasma Sour. Sci. Technol.*, vol. 16, no. 4, pp. R1–R25, 2007.

[27] D. M. Goebel and I. Katz, "Fundamentals of electric propulsion: Ion and Hall thrusters," Jet Propuls. Lab., California Inst. Technol., Pasadena, CA, USA, Tech. Rep., 2008.

[28] H. J. Leiter, R. Killinger, H. Bassner, J. Müller, and R. Kukies, "Development of the radio frequeny ion thruster RIT XT—A status report," in *Proc. 27th Intern. Elect. Propuls. Conf.*, 2001, pp. 1–8.

Roberto A. Dextre received the B.S. degree in mechanical and aerospace engineering from SUNY Binghamton, Binghamton, NY, USA, in 2012, and the M.S. degree in mechanical and aerospace engineering from The University of Alabama in Huntsville, Huntsville, AL, USA, in 2014, where he is currently pursuing the Ph.D. degree with the Mechanical and Aerospace Engineering Department.

His current research interests include plasma propulsion and microwave microplasma physics.

Kunning G. Xu (M'13) received the B.S., M.S., and Ph.D. degrees in aerospace engineering from the Georgia Institute of Technology, Atlanta, GA, USA, in 2006, 2009, and 2012, respectively.

Since 2012, he has been an Assistant Professor with the Mechanical and Aerospace Engineering Department, University of Alabama in Huntsville, Huntsville, AL, USA. His current research interests include plasma propulsion, plasma assisted combustion, and atmospheric-pressure microplasma physics.

Dr. Xu is a member of AIAA and AVS.